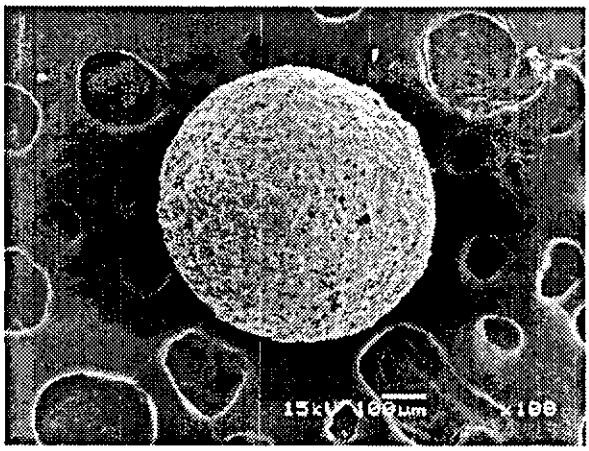

Fig. 1. Porous beads composed of TCP (Bar: μm).

bubble was introduced into the slurry [6]. Then the slurry was dropped into liquid nitrogen dropwise. The slurry drops were frozen and freeze-dried. The beads were then sintered at 1100 °C for 10 h. After etching in acetic acid (0.1 N), porous beta tricalcium phosphate (beta TCP) beads were formed (Fig. 1).

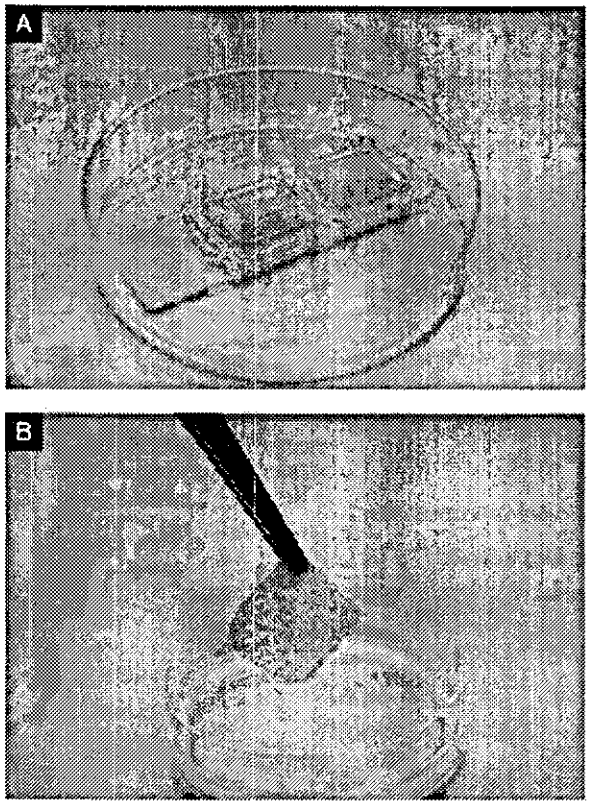

Fig. 2. Preparation of bead–cell sheets. (A) A mold, (B) a bead–cell sheet cultured.

Table 1
Formation ratio of bead–cell sheet (the shape of molds was a circle)

Inoculation number (cells/4 cm^2)	Probability of success formation (%)
10^6 cells	80
10^7 cells	83
10^8 cells	0

2.2. Cell isolation and culture

Bone marrow was obtained from tibiae and femora of 2–3-week-old bovine calves. The contents of the bone marrow cavities were aseptically harvested in alpha-modified Eagle's medium (alpha-MEM), single-cell suspension was made by passing the marrow through 20-gauge needles three times, and cells were resuspended in alpha-MEM supplemented with 10% fetal bovine serum, 100 U/ml penicillin and 100 mg/l streptomycine (P/S). Nucleated cells were cultured in a humidified 37 °C/5% CO_2 incubator. Bone marrow stromal cells (BMSCs) were selected based on their ability to adhere to the Petri dish; nonadherent hematopoietic cells were removed with the medium during refeeding [7,8]. The medium was completely replaced after 3 days and twice per week thereafter. When BMSCs became about 80% confluent (approximately 2–3 weeks after the primary culture was established), they were detached using 0.25% trypsin/1 mM ethylenediamine tetraacetic acid and replated in 100-mm dishes at 5×10^3 cells/cm^2. After one more week, when the dishes were fully confluent, second passage (P2) cells were removed with the trypsin solution and seeded onto a mold with porous beads.

2.3. Preparation for a bead–cell sheet

Expanded BMSCs were seeded to a mold with porous beads composed of beta-TCP and incubated with alpha-MEM. As a differentiation medium for bone, we used Dulbecco's MEM (DMEM) supplemented with 10% fetal bovine serum, 0.1 mM nonessential amino acids, 50 μg/ml ascorbic acid, P/S, 100 nM dexamethasone, and 5 μg/ml insulin, and 7 mM beta-glycerophosphate.

3. Results

For a fabrication of a bead–cell sheet, we first investigated whether or not there is a desirable ratio between the number of beta-TCP beads and BMSCs by

Table 2
Formation ratio of bead–cell sheet (the shape of molds was a quadrangle)

Inoculation number (cells/cm^2)	Probability of success formation (%)
0.2×10^6 cells	50
0.2×10^7 cells	75
0.2×10^8 cells	0

using two kinds of molds having circle and quadrangle shapes. If the cell number is too small, each bead cannot be connected with each other due to small amount of connective matrix (collagen, fibronectin, etc) produced by the cells. When 10^6, 10^7, and 10^8 cells were inoculated to the bottom surface of quadrangle-shaped molds (20×20 mm, Fig. 2A) whose bottom surface were covered with beta-TCP beads as a monolayer, the formation ratio of the bead–cell sheets was examined. In the case of 10^6 or 10^7 cells, it was found that the bead–cell sheet was successfully formed and the probabilities of success formation after 24 h were 80% ($n=10$) and 83% ($n=6$), respectively (Table 1). However, the inoculation number of the 10^8 cells ($n=1$) to the mold reduced the probability of ratio to 0%.

In the same way, a mold with a circle shape having an area of 1 cm^2 was also prepared in order to form a bead–cell sheet. An inoculum size of 0.2×10^6 cells resulted in a low successful probability ($n=4$) of the sheet formation as shown in Table 2. In the case of 0.2×10^7 cells, the ratio was 75% ($n=4$). On the other hand, inoculation number of 0.2×10^8 cells had failures in the formation of the bead–cell sheet ($n=1$), presumably because the high inoculation density of the cells might bring shortages of oxygen and nutrition. From the results of Tables 1 and 2, it was found that ranges in an inoculation densities between 0.25×10^6 and 0.25×10^7 cells/cm^2 were optimum for the successful formation of bead–cell sheets.

Because the sheet formed in an expansion culture medium was so fragile, the construct was hardly manipulated without reinforcement. Therefore, a long-term culture (7 days) of the bead–cell sheet was performed in vitro in a differentiation culture medium supplemented with several factors to induce the production of bone matrices from BMSCs seeded into the beta-TCP beads. As the result, we could easily manipulate the bead–cell sheet with tweezers (Fig. 2B). Addition of poundage on the overlain cell–bead sheets induced the connection of these sheets with each other and achievement of thicker implant formation. A nonwoven fiber fabric sheet of poly-L-lactic acid (PLLA) could also be inserted in between each cell–bead sheet. Consequently, bone implants having a size of $20 \times 20 \times 5$ mm were successfully developed. Because the bead–cell sheet could adhere to other scaffolds such as a nonwoven fiber sheet of PLLA (Fig. 3), it was suggested that if we make the implant having a large size, include cells until the center of the scaffold.

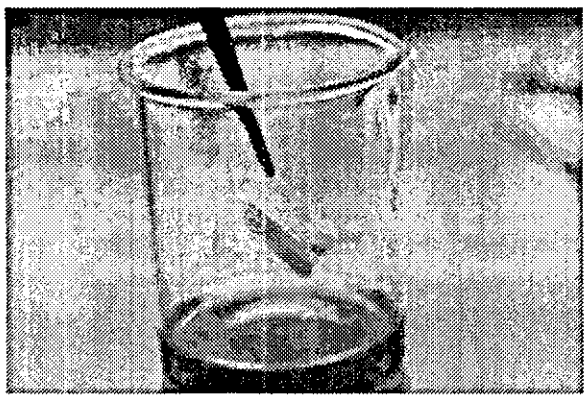

Fig. 3. Implant piled the bead–cell sheets and nonwoven fiber fabric sheets of PLLA up for bone tissue engineering.

4. Discussion

To make artificial bone implants with a larger size composed of osteoprogenitor cells, we newly developed a bead–cell technology. The techniques developed in this study, i.e., piling up cell–bead sheets to make a thicker construct, realized the formation of a larger bone implant with a size of at least $20 \times 20 \times 5$ mm than that of previously reported ones [5,6]. Some problems previously suggested such as insufficient seeding efficiency of the cells to the center of scaffolds may be resolved in our model because the implant is assembled in vitro by piling up the bead–cell sheets just before implantation to an animal. Short-time culture after composition of the each element, cell–bead sheets and/or biodegradable polymer sheets, would prevent necrosis at the center of the implant. In our model, rapid angiogenesis to the implant after transplantation is needed, and the speed of the angiogenesis into the central space of the implant may determine the size of implant itself. The maximum (optimum) size may also change dependently on site of the transplant in a body, because, for example, a well-vascularized tissue has higher oxygen content. Further research should be done in order to determine the limitation in the size of the implant.

A nonwoven fiber fabric of PLLA was used to prevent necrosis in a central space of the implants. Because the PLLA fabric is a highly porous biodegradable scaffold, a tissue fluid enriched with oxygen and nutrition should easily be introduced into their interspaces, thereby inducing rapid angiogenesis in the construct. A design and a selection for the biodegradable scaffold in our model should be taken into consideration according to the speed of angiogenesis and the tactical degradation time of the biodegradable polymer, the latter of which can make a space for the development of vasculature and regeneration of bone tissue.

In our method, a shape of the sheet could be changed depending on the shape of the bone defect. From the result of Tables 1 and 2, it was confirmed that the sheet with a shape of circle and quadrangle can be formed with ease. Therefore, by piling up the bead–cell sheets, a three-dimensional bone implant which, we hope, might also be also able to be prepared. Therefore, this kind of technique should also be useful in engineering thick implants for other tissue.

5. Conclusions

We developed a new tissue-engineered bone graft model composed of BMSCs and beta TCP porous beads. Cell–bead sheets prepared by means of cultivation of BMSCs with the beads induced the connection of these sheets with each other and resulted in thicker implant formation. Therefore, our new model should become an important one for tissue engineering put into a target of particularly focusing on implants with larger and complicated structures.

Acknowledgements

This work was partly supported by a Grant-in-Aid from the Japanese Ministry of Education, Science and Culture.

References

[1] H. Yoshikawa, H. Ohgushi, H. Nakajima, E. Yamada, K. Ichijima, S. Tamai, T. Ohta, Transplantation 69 (2000) 128–134.
[2] S. Rao, K.S. Furukawa, T. Mizumi, T. Ushida, T. Tateishi, Mater. Sci. Eng., C, Biomim. Mater., Sens. Syst. 17 (2001) 113–117.
[3] T. Ushida, K.S. Furukawa, K. Toita, T. Tateishi, Cell Transform. 11 (2002) 489–494.
[4] J. Goshima, V.M. Goldberg, A.I. Caplan, Clin. Orthop. 262 (1991) 298–311.
[5] M. Akahane, H. Ohgushi, T. Yoshikawa, T. Sempuku, S. Tamai, S. Tabata, Y. Dohi, J. Bone Miner. Res. 14 (4) (1999) 561–568.
[6] T. Ushida, G. Chen, T. Tamaki, Y. Umezu, T. Tateishi, Bioceramics 13 (2001) 519–522.
[7] I. Martin, V.P. Shastri, R.F. Padera, J. Yang, A.J. Mackay, R. Langer, G. Vunjak-Novakovic, L. Freed, J. Biomed. Mater. Res. 55 (2001) 229–235.
[8] H. Suenaga, K.S. Furukawa, T. Ushida, T. Takato, T. Tateishi, Materials Science C (in press).

Available online at www.sciencedirect.com

SCIENCE DIRECT®

Materials Science and Engineering C 24 (2004) 875–879

MATERIALS SCIENCE & ENGINEERING C

www.elsevier.com/locate/msec

Novel bone graft model using bead-cell sheets composed of tricalcium phosphate beads and bone marrow cells

Shunsuke Miyauchi[a], Katsuko S. Furukawa[a,*], Yoshikazu Umezu[b], Yasuyuki Ozeki[b], Takashi Ushida[a,c], Tetsuya Tateishi[d]

[a]*Biomedical Engineering, Laboratory, Department of Mechanical Engineering, Graduate School of Engineering, University of Tokyo, 503, 8th Building, 7-3-1 Hongo, Bunkyo, Tokyo 113-8656, Japan*

[b]*Advance Co., Saitama, Japan*

[c]*Division of Biomedical Materials and Systems, Center for Disease Biology and Integrative Medicine, School of Medicine, The University of Tokyo, Japan*

[d]*Biomaterials Center, National Institute for Materials Science, Ibaraki, Japan*

Received 20 June 2004; received in revised form 16 July 2004; accepted 16 July 2004

Abstract

Cells on scaffold implanted in vivo need nutrient and oxygen carried on the blood stream. In this respect, many scaffolds consisting of porous ceramics cannot hold cells alive in the center of them. Therefore, osteogenesis and substitution of regenerated bone occur from the surface of graft, and the biodegradation speed is slow. To solve this problem of lack of blood stream, we developed a new bone graft sheet composed of human bone marrow stromal cells (HMSCs), and beta-tricalcium phosphate (beta-TCP) porous beads. In addition, by combining multilayered bead-cell sheets and collagen gel, we fabricated a bone graft having the space for entry of blood vessels, and implanted them subcutaneously in mice. After 3 weeks, blood vessels reaching to the focal area of graft were recognized, and near the surface of graft, osteogenesis was also observed. In conclusion, the bead-cell sheet would have good osteoconductivity, and the graft made of bead-cell sheets showed a new design concept of bone graft preparing the space for neovascularization.

Keywords: Bone tissue engineering; Sheet; Bead; Bone marrow cell

1. Introduction

Recently, the need for establishment of treatments of bone defects is increasing. Because of the risk of immunologic rejection, the use of allogeneic and xenogeneic bone as a substitute is limited. In addition, a series of large bone defects caused severe difficulties in using autologous tissue [1]. Thus, artificial bones composed of metals such as aluminum, stainless, or titanium have been applied for the patients, but these implants also have many problems. Metal-based artificial bones have inappropriate mechanical properties that differ from those of natural bones, inducing abrasion, attrition, and absorption in the original bone of the patients around the implanted artificial bone [2]. From these facts, the development of tissue-engineered artificial bones similar in mechanical properties of natural bones is expected.

In the field of bone tissue engineering, there is a limitation in the size of the implant. When we had an attempt to make a bone implant with larger sizes, it was difficult to realize homogenous inoculation of the cells, particularly in the center of the scaffold [3]. Even if cells could be successfully inoculated a lot of cells into the center of the scaffold, necrosis may develop most often in the center due to limitations in diffusion of the oxygen and nutrition. Therefore, the present study was designed to make

* Corresponding author. Tel.: +81 3 5841 6331; fax: +81 3 5841 6442.
E-mail address: furukawa@mech.t.u-tokyo.ac.jp (K.S. Furukawa).

0928-4931/$ - see front matter © 2004 Elsevier B.V. All rights reserved.
doi:10.1016/j.msec.2004.08.031

a new bone implant that has a larger size than that of a previously reported one [4,5], and a large number of alive cells even in the center of the implant.

To prevent necrosis and keep cells in the center of implant, blood stream near the cells is necessary. In this viewpoint, we had developed a new tissue-engineered bone graft sheet composed of human bone marrow stromal cells (HMSCs), and beta-tricalcium phosphate (beta-TCP) porous beads [6]. These sheets had been layered and adhered non-woven fiber sheets of poly-L-lactic acid (PLLA). Then, a large bone graft model (the size was approximately 20×20×5 mm) having a spongy layer for diffusion of nutrition had been fabricated. That model could have kept cells inside, even in the center, and the necrosis had not occurred. The result of our model had suggested a new bone implant design to multilayer the cell-sheet and nutrient diffusion space.

In this study, we developed a new bone graft as a result of expanding concept of nutrient supply and consideration of the possibility of invasion of newly generated blood vessels.

2. Materials and methods

2.1. Preparation of porous beads composed of calcium phosphates

Aqueous slurry of calcium phosphates and a binder reagent were mixed in an ultrasonic homogenizer and air bubble was introduced into the slurry [7]. Then the slurry was dropped into liquid nitrogen drop-wise. The slurry drops were frozen and freeze-dried. The beads were then sintered at 1100 °C for 10 h. After etching in acetic acid (0.1 N), porous beta-tricalcium phosphate (beta-TCP) beads were formed (Fig. 1).

2.2. Cell isolation and culture

Bone marrow (25 ml) was obtained by posterior iliac crest from normal human donors (ages 18–45 years) by board-certified physicians. HMSCs were isolated from these marrow aspirates using methods modified from those described previously [8]. Briefly, 25 ml of marrow was added to 15 ml of phosphate-buffered saline (PBS) and 125 U heparin/ml, and centrifuged to pellet the cells and remove the fat layer. The remaining nucleated cells were plated at 1×10^8 nucleated cells/500 cm^2 dish containing 80 ml of medium. The medium consisted of DMEM supplemented with 10% fetal bovine serum, 1 ng/ml recombinant fibroblast growth factor, and antibodies (100 U/ml penicillin, 100 μg/ml streptomysin sulfate and 0.25 μg/ml amphotericin B; GIBCO, US). The HMSCs were cultured at 37 °C in a humidified atmosphere containing 95% air and 5% CO_2. The medium was renewed twice a week, and floating cells were removed when the medium was changed. Thus, the adherent HMSCs were selectively obtained. When HMSCs became about 80% confluent, they were detached using 0.25% trypsin/1 mM EDTA and replated at 5×10^3 cells/cm^2. After one more week, when the dishes were fully confluent, second passage (P2) cells were removed and seeded onto a mold with porous beads at a cell density 2.5×10^5 cells/cm^2.

2.3. Preparation for a bead-cell sheet

Expanded HMSCs were seeded to a mold (cell density is 2.5×10^5 cells/cm^2) with porous beads composed of beta-TCP (diameter; 300 μm) and incubated with Dulbecco's MEM (DMEM). As osteogenic induction medium, we used DMEM supplemented with 10% fetal bovine serum, 100 nM dexamethasone, 10 mM beta-glycerophosphate, 0.05 mM ascorbic acid, and 1 ng/ml b-fibroblast growth factor (b-FGF) [9].

2.4. Alizarin Red S and alkaline phosphatase staining of a bead-cell sheet

For the Alizarin Red S staining, the bead-cell sheet was washed with PBS (−) (phosphate-buffered saline without Ca^{2+} and Mg^{2+}) and fixed with 95% ethanol (5

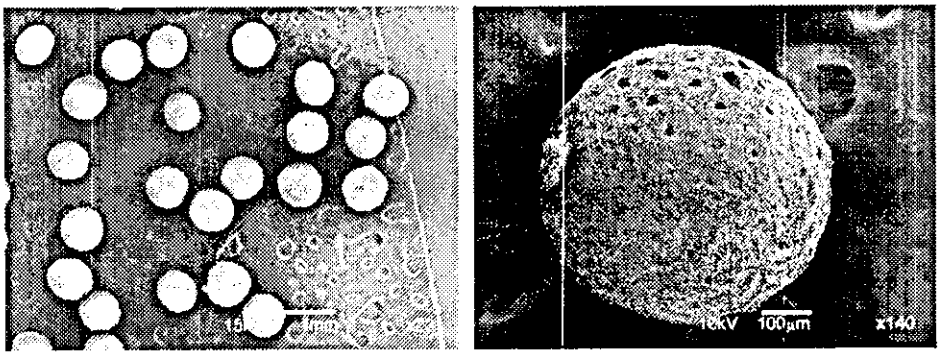

Fig. 1. TCP porous beads.

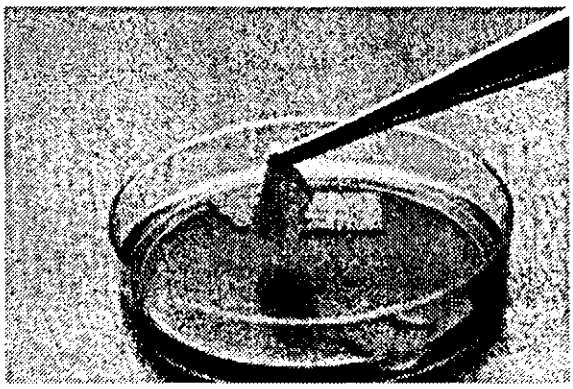

Fig. 2. Bead-cell sheets.

min). Then the sheet was washed deionized water, and Alizarin Red S (Wako) solution was added to the cultured well. After 2 min, the sheet was washed several times with deionized water to remove the remaining stain.

For the alkaline phosphatase (ALP) staining, the sheet was washed with PBS (−), and then fixed and stained with leukocyte alkaline phosphatase staining kit (Sigma Diagnostics). Briefly, the bead-cell sheet was fixed with citrate concentrated solution and acetone (30 s). Then, the alkaline–dye mixture, which consisted of 2 ml Naphthol AS-MX phosphate alkaline solution (0.25% Naphthol AS-MX phosphate, buffered at pH 8.6) and 12 mg of fast blue RR salt dissolved in 48 ml of deionized water, was added. The sheet was incubated at room temperature for 30 min, and then washed several times with deionized water to remove the remaining stain.

2.5. In vitro long-term culture

By combining multilayered six bead-cell sheets with collagen gel, a bone graft was fabricated. The size of graft was approximately 2×2×1 cm. Collagen gel was prepared by mixing collagen type I (KOKEN, Japan) with 10% DMEM, 10% $NaHCO_3$, and 2% [4-(2-hydroxyethyl)-1-piperazinyl]ethanesulfonic (HEPES). Including controls, following eight kinds of graft model were prepared; (1) bead-cell sheet and collagen gel, (2) bead-cell sheets, collagen gel, and human umbilical vein endothelial cells (HUVEC) in the gel, (3) collagen gel, (4) collagen gel and HUVEC in the gel, (5) bead-cell sheets, (6) beta-TCP beads, collagen gel, and HMSCs in the gel, (7) beta-TCP beads, collagen gel, and HUVEC and HMSCs in the gel, (8) collagen gel and HMSCs in the gel.

These grafts were cultured in vitro for 2 months, and the change in shape of the grafts was observed to investigate the effects of bead-cell sheets on the shape of graft.

2.6. Implantation and harvest

To evaluate the competency of the implants such as inductivity of blood vessels and osteoconductivity, implanting experiment was done. Athymic nude male mouse was obtained at 5 weeks and acclimated for 2 weeks before use. Diethyl ether was used for anesthesia. In this experiment, we prepared four kinds of graft. The size was approximately 1×1×1 cm. The grafts were composed of (A) bead-cell sheets and collagen gel, (B) bead-cell sheets, collagen gel, and HUVEC in the gel, (C) collagen gel, and (D) beta-TCP beads, collagen gel,

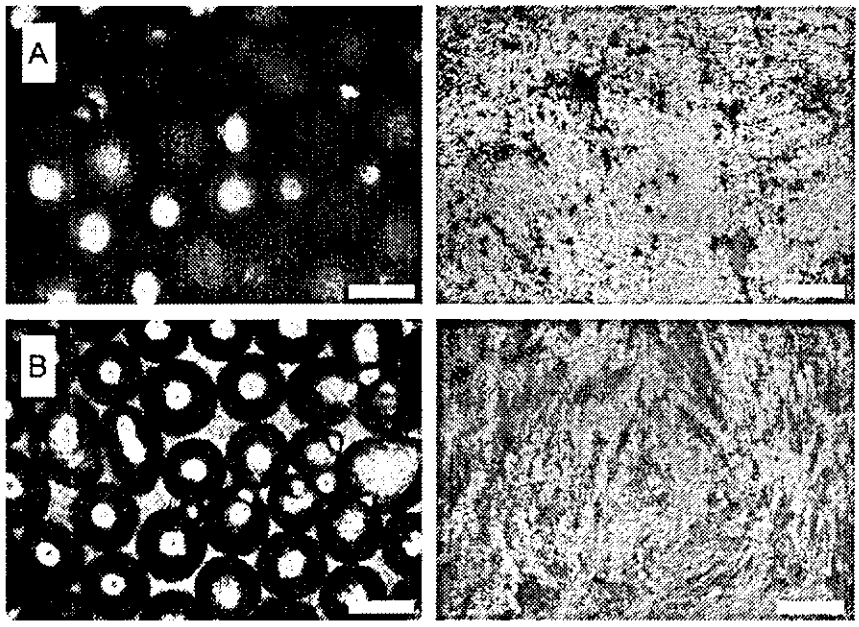

Fig. 3. Alizarin Red S (A) and ALP staining (B) of bead-cell sheet (left) and monolayer (right) (scale bars: 300 μm).

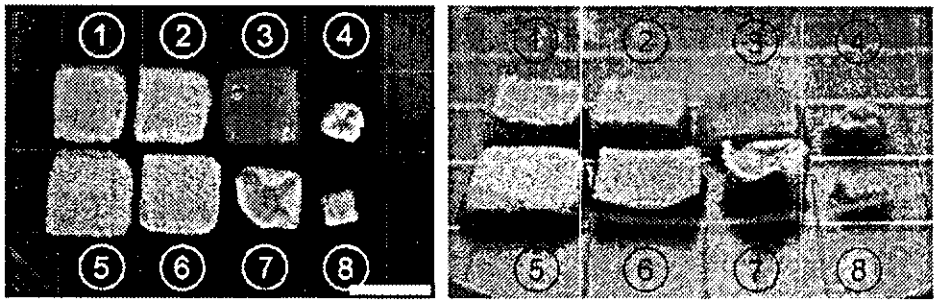

Fig. 4. Implants after long-term incubation in vitro. ① Bead-cell sheet and collagen gel, ② bead-cell sheets, collagen gel, and HUVEC in the gel, ③ collagen gel, ④ collagen gel and HUVEC in the gel, ⑤ bead-cell sheets, ⑥ beta-TCP beads, collagen gel, and HMSCs in the gel, ⑦ beta-TCP beads, collagen gel, and HUVEC and HMSCs in the gel, ⑧ collagen gel and HMSCs in the gel (scale bar: 2 cm).

and HMSCs in the gel. They were implanted subcutaneously in the dorsum of athymic nude mice (two samples/mouse). The implants were harvested after 3 weeks.

The implanted samples were fixed in 10% neutral-buffered formalin solution, and embedded in paraffin, and sectioned (10 μm thick). The cross-sections were stained with hematoxylin and eosin, and elastica van Gieson stain (EVG).

3. Results

After 2 weeks of incubation in osteogenic induction medium, the bead-cell sheet had enough strength to be manipulated with tweezers (Fig. 2).

Alizarin Red S staining of the bead-cell sheet after 2 weeks revealed that more calcium was detected in bead-cell sheet than in monolayer as a control (Fig. 3A). Similarly, ALP staining showed that ALP activity increased in bead-

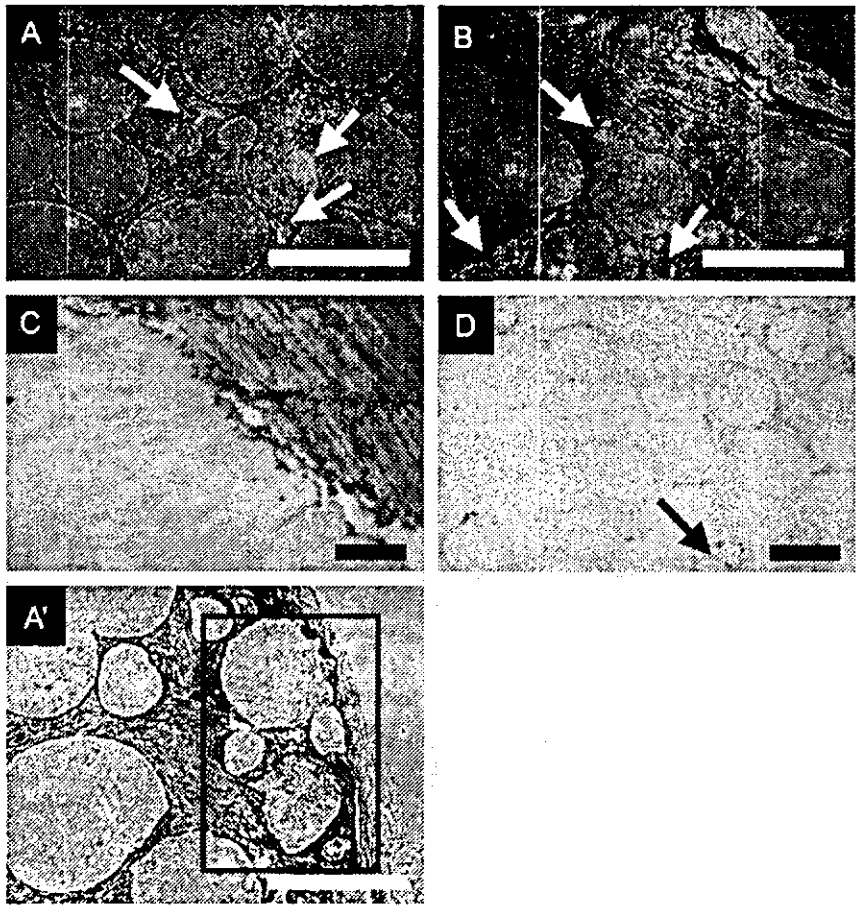

Fig. 5. Comparison of implant (A) bead-cell sheets and collagen gel, (B) bead-cell sheets, collagen gel, and HUVEC in the gel, (C) collagen gel, and (D) beta-TCP beads, collagen gel, and HMSCs in the gel (scale bars: 300 μm). Arrows indicate blood vessels. (A′) shows osteogenesis.

cell sheet than that in monolayer (Fig. 3B). Because these dyes stained strongly with beta-TCP beads, glass beads (diameter; 300 μm) were used here to decrease background.

As shown in Fig. 4, the grafts after the incubation of 2 months in vitro showed the change in shape. Grafts not including bead-cell sheets, sample numbers 4, 6, 7, and 8, shrank. Especially grafts 4 and 8 shrank to almost one-fourth of graft 3, which did not include cells. On the other hand, grafts 1, 2, and 5 including bead-cell sheets had been holding the original size and shape.

Histological examination of implanted samples to nude mice using hematoxylin and eosin stains revealed that red blood cells in blood-vessel-like tissues existed in the central area of grafts A and B (Fig. 5A,B). By EVG staining, it was verified that the cells were red blood cells. In grafts C and D, the blood vessel-like tissues were scarcely observed as shown in Fig. 5C,D. In the area near the surface of graft A, osteogenesis was recognized (Fig. 5A′). In addition, similar tissue was observed in graft B. But in grafts C and D, no osteogenesis was recognized.

4. Discussion

In tissue engineering approach, bone marrow stromal cells (MSCs) have been used in condition that they were loaded with porous scaffolds, such as ceramics [8]. It is difficult to seed cells to the central area of these scaffolds, and if seeded, cells cannot be alive without the blood stream, and then necrosis occurs. Because of the necrosis, cells exist only in the area near the surface of scaffolds. Therefore, these porous scaffolds are degraded from the surface, but not from inside. This problem of difficulty to hold cells inside affects the slowness in degradation speed.

An ideal scaffold in bone repair has following three properties; (1) holding cells in the focal area of the graft, (2) inducing blood vessels into the graft, and (3) being degraded to regenerated bone. In our model, cells in the bead-cell sheet were considered to differentiate for osteoblasts from the increasing of calcium and ALP activity. The bead-cell sheet could hold cells inside homogeneously, and as shown in result of long-term culture in vitro, it would have enough strength to keep the shape. These characteristics of bead-cell sheet were useful to fabricate the graft holding cells inside.

Histological observation with hematoxylin and eosin staining revealed that blood vessel-like tissues entered into the focal area of the implant samples. With EVG staining, red blood cells in those blood vessel-like tissues were observed. These facts would be enough to prove these tissues to be vascularized. Therefore, it was suggested that our new model for bone graft had ideal property, as discussed above inductivity for blood vessels.

Histological observation with HE staining also revealed that osteogenesis occurred in the subcutaneous implantation. This result suggested the high osteoconductivity of the implants. From these results, the implants fabricated were considered to satisfy the ideal properties required for bone graft as discussed above. However, osteogenesis was not observed in the focal area. Thus, newly generated bone near the surface might be derived from host mouse. In addition, bone graft should be substituted by regenerated bone and involved to the bone remodeling. From the viewpoint, short-term implantation of 3 weeks is not adequate. Longer-term implantation should be done to verify whether the blood stream affects the osteogenesis or not.

5. Conclusions

The implants fabricated with multilayered bead-cell sheets and collagen gel were considered to keep the cells homogeneously inside of them. They showed a good inductivity for blood vessels and osteoconductivity in the experiments of subcutaneous implantation in nude mice.

References

[1] H. Yoshikawa, H. Ohgushi, H. Nakajima, E. Yamada, K. Ichijima, S. Tamai, T. Ohta, Transplantation 69 (2000) 128–134.
[2] S. Rao, K.S. Furukawa, T. Mizumi, T. Ushida, T. Tateishi, Mater. Sci. Eng., C, Biomim. Mater., Sens. Syst. 17 (2001) 113–117.
[3] T. Ushida, K.S. Furukawa, K. Toita, T. Tateishi, Cell Transplant 11 (2002) 489–494.
[4] J. Goshima, V.M. Goldberg, A.I. Caplan, Clin. Orthop. 262 (1991) 298–311.
[5] M. Akahane, H. Ohgushi, T. Yoshikawa, T. Sempuku, S. Tamai, S. Tabata, Y. Dohi, J. Bone Miner. Res. 14 (4) (1999) 561–568.
[6] K.S. Furukawa, S. Miyauchi, D. Suzuki, Y. Umezu, T. Shinjo, T. Ushida, M. Eguchi, T. Tateishi, Mater. Sci., C 24 (2004) 437–440.
[7] T. Ushida, G. Chen, T. Tamaki, Y. Umezu, T. Tateishi, Bioceramics 13 (2001) 519–522.
[8] S.E. Haynesworth, J. Goshima, V.M. Goldberg, A.I. Caplan, Bone 13 (1992) 81–88.
[9] N. Jaiswal, S.E. Haynesworth, A.I. Caplan, S.P. Bruder, J. Cell. Biochem. 64 (1997) 295–312.

THE JOURNAL OF BIOLOGICAL CHEMISTRY
© 2004 by The American Society for Biochemistry and Molecular Biology, Inc.

Vol. 279, No. 27, Issue of July 2, pp. 28789–28797, 2004
Printed in U.S.A.

Methylation in the Core-promoter Region of the Chondromodulin-I Gene Determines the Cell-specific Expression by Regulating the Binding of Transcriptional Activator Sp3*

Received for publication, February 4, 2004, and in revised form, April 5, 2004
Published, JBC Papers in Press, April 23, 2004, DOI 10.1074/jbc.M401273200

Tomoki Aoyama‡§, Takeshi Okamoto‡§, Satoshi Nagayama¶, Koichi Nishijo‡§, Tatsuya Ishibe‡§, Ko Yasura‡, Tomitaka Nakayama§, Takashi Nakamura§, and Junya Toguchida‡‖

From the ‡Institute for Frontier Medical Sciences, Kyoto University, Kyoto 606-8507, Japan, the §Department of Orthopedic Surgery, Graduate School of Medicine, Kyoto University, Kyoto 606-8507, Japan, and the ¶Department of Surgical Oncology, Graduate School of Medicine, Kyoto University, Kyoto 606-8507, Japan

Transcriptional regulation of cell- and stage-specific genes is a crucial process in the development of mesenchymal tissues. Here we have investigated the regulatory mechanism of the expression of the chondromodulin-I (*ChM-I*) gene, one of the chondrocyte-specific genes, in osteogenic cells using osteosarcoma (OS) cells as a model. Methylation-specific sequence analyses revealed that the extent of methylation in the core-promoter region of the *ChM-I* gene was correlated inversely with the expression of the *ChM-I* gene in OS primary tumors and cell lines. 5-Aza-deoxycytidine treatment induced the expression of the *ChM-I* gene in ChM-I-negative OS cell lines, and the induction of expression was associated tightly with the demethylation of cytosine at −52 (C(−52)) in the middle of an Sp1/3 binding site to which the Sp3, but not Sp1, bound. The replacement of C(−52) with methyl-cytosine or thymine abrogated Sp3 binding and also the transcription activity of the genomic fragment including C(−52). The inhibition of *Sp3* expression by small interfering RNA reduced the expression of the *ChM-I* gene in ChM-I-positive normal chondrocytes, indicating Sp3 as a physiological transcriptional activator of the *ChM-I* gene. These results suggest that the methylation status of the core-promoter region is one of the mechanisms to determine the cell-specific expression of the *ChM-I* gene through the regulation of the binding of Sp3.

Chondromodulin-I (ChM-I)[1] is a 25-kDa glycoprotein originally purified from bovine epiphyseal cartilage on the basis of growth-promoting activity for chondrocytes (1) and subsequently revealed to be a potent vascular endothelial cell growth inhibitor (2). During embryonal development, the expression of the *ChM-I* gene is first observed in all of the cartilaginous tissues, which are composed of prehypertrophic chondrocytes (3). As the development proceeds, hypertrophic chondrocytes develop in the center of cartilaginous bone rudiments where the expression of the *ChM-I* gene shows a marked decrease (3). No expression of the *ChM-I* gene is observed in bone tissues developing after vascular invasion in the area adjacent to hypertrophic chondrocytes (3). In matured limbs, the expression of the *ChM-I* gene is limited to cells in the resting, proliferating, and early hypertrophic zone of the growth plate (2–4). These results suggest that the expression of the *ChM-I* gene is regulated strictly in a cell- and stage-related manner, although the molecular mechanisms leading to this spatiotemporal expression have not been elucidated.

Osteosarcoma (OS) is defined as a sarcoma that produces a bone matrix called osteoid, suggesting that the precursor cells of OS are cells of the osteogenic lineage (5). The degree of differentiation as osteoblasts, however, differs considerably among OS ranging from tumors with a large amount of osteoid and expressing a number of bone-related genes such as alkaline phosphatase (*ALP*) and osteocalcin (*OCN*) genes, namely osteoblastic OS (OBOS), to tumors in which an osteoid is hardly seen, fibroblastic OS (FBOS) (6–8). A particular intriguing subtype of OS is chondroblastic OS (CBOS) in which tumor cells directly produce immature cartilage in addition to osteoid (5, 9), suggesting that tumor cells in this subtype have the potential to differentiate into both osteogenic and chondrogenic cells. These clinical findings suggest that the precursor cells of OS range from mesenchymal stem cells to mature osteoblasts and that OS cells can be used as materials to investigate the regulatory mechanisms of cell- and stage-specific genes such as the *ChM-I* gene.

Here we first analyzed the expression of the *ChM-I* gene in primary OS tumors and cell lines and found that the gene was expressed strongly in CBOS but not in tumors of other subtypes. This result prompted us to investigate the involvement in regulation of the expression of the *ChM-I* gene of an epigenetic mechanism, which has been studied extensively as the mechanism controlling the expression of cell- and stage-specific genes (10). We found that the expression of the *ChM-I* gene was regulated positively by a transcription factor, Sp3, and that the binding of Sp3 was regulated by the methylation status in the core-promoter region of the *ChM-I* gene, especially at one Sp3 binding site.

EXPERIMENTAL PROCEDURES

Tissue Samples—Primary tumor tissues from 24 OS cases were obtained at either biopsy or resection. All were conventional high grade tumors, and histological subtypes were OBOS in 13 cases, CBOS in 6 cases, and FBOS in 5 cases. Tumor specimens were frozen quickly and kept at −80 °C until nucleic acid extraction. As a control of the expres-

* This work was supported in part by grants-in-aid for Scientific Research from the Japan Society for the Promotion of Science and from the Ministry of Health, Labor, and Welfare of Japan. The costs of publication of this article were defrayed in part by the payment of page charges. This article must therefore be hereby marked "*advertisement*" in accordance with 18 U.S.C. Section 1734 solely to indicate this fact.

‖ To whom correspondence should be addressed: Institute for Frontier Medical Sciences, Kyoto University, 53 Kawahara-cho, Shogoin, Sakyo-ku, Kyoto 606-8507, Japan. Tel.: 81-75-751-4134; Fax: 81-75-751-4144; E-mail: togjun@frontier.kyoto-u.ac.jp.

[1] The abbreviations used are: ChM-I, chondromodulin-I; OS, osteosarcoma; OBOS, osteoblastic OS; FBOS, fibroblastic OS; CBOS, chondroblastic OS; 5-Aza-dC, 5-aza-2-deoxycytidine; RT, reverse transcription; siRNA, small interfering RNA; ChIP, chromatin immunoprecipitation; AGC, aggrecan.

sion of the *ChM-I* gene, total RNA was extracted from the articular cartilage of the ankle joint of an 11-year-old male who underwent an above-knee amputation because of osteosarcoma of the femur.

Cell Culture and Reagents—The human osteosarcoma cell lines Saos2, HuO, HOS, MG63, and U2OS were obtained from either ATCC or the Japanese Cancer Research Resources Bank. The human osteosarcoma cell line TAKAO is a clonal cell line derived from SU cells (11). ANOS was established in our laboratory using material from a 12-year-old female with CBOS. These cell lines were maintained in Dulbecco's modified Eagle's medium with 10% heat-inactivated fetal bovine serum. Chondrocytes were isolated from articular cartilage tissue from the ankle joint of an 11-year-old male who underwent an above-knee amputation because of a malignant bone tumor of the femur. *Drosophila* SL2 cells were kindly provided by T. Uemura and maintained in Schneider's insect medium supplemented with 10% fetal bovine serum at 25 °C in room temperature. In the demethylation experiments, cells were treated with 5-aza-2-deoxycytidine (5-Aza-dC, Sigma) for 5 days.

Reverse Transcription (RT)-PCR—RNA was isolated using TRIzol reagent (Invitrogen) from frozen tumor tissues and cell lines. All of the RT reactions were performed using 1 μg of total RNA with the SuperScript first strand synthesis system for the RT-PCR kit (Invitrogen). PCR was performed in duplicate for each sample using primers specific for *ChM-I* (sense, 5′-CATCGGGGCCTTCTACTTCT-3′; antisense, 5′-GGCATGATCTTGCCTTCCAG-3′, length 312 bp) (12), *Sp1* (sense, 5′-CTACCCCTACCTCAAAGGAAC-3′; antisense, 5′-CTCTCCTTCTTTTTGCTGGCCT-3′, length 821 bp) (13), and *Sp3* genes (sense, 5′-TTCAGGGAGTTGCAATTGGTG-3′; antisense, 5′-TTCTGTGCCTGTGTCTCTTCA-3′, length 448 bp) (13). The PCR products were loaded on 1.5% agarose gel and visualized by ethidium bromide staining.

Quantitative RT-PCR of the ChM-I Gene—The relative amount of *ChM-I* mRNA was assessed by TaqMan real-time PCR with the ABI PRISM 7700 sequence detection system (PE Applied Biosystems). A 75-bp fragment from +411 (exon 4) to +485 (exon 5) of the *ChM-I* cDNA (GenBank™ accession number XM_007132) was amplified using specific primers (sense, 5′-GAAGGCTCGTATTCCTGAGGTG-3′; antisense, 5′-TGGCATGATCTTGCCTTCCAGT-3′) and labeled with a TaqMan probe (5′-FAM-CGTGACCAAACAGAGCATCTCCTCCA-3′-TAMRA). 18 S rRNA was used as the internal control, and all of the reactions were run in duplicate. The ratio of *ChM-I*/18 S in each sample was calculated, and the expression level of *ChM-I* genes was demonstrated as a relative value using the *ChM-I*/18 S ratio in human articular cartilage as a standard (1.0).

Western Blotting—Whole cell lysates were prepared from each cell line, separated by SDS-PAGE using 10% polyacrylamide gel, and transferred to a nitrocellulose membrane (Millipore). The membrane was treated with a primary antibody at an appropriate dilution and then with goat anti-rabbit IgG antibody conjugated to horseradish peroxidase as a secondary antibody (Dako) and visualized using an ECL plus kit (Amersham Biosciences). The antibody for the human ChM-I protein was kindly provided by Y. Hiraki. Antibodies for Sp1 and Sp3 were purchased from Santa Cruz Biotechnology (Santa Cruz, CA).

Bisulfite Genomic Sequencing—The conversion of non-methylated cytosine residues to uracils in genomic DNA was performed with bisulfite as described previously (14). One microgram of genomic DNA extracted from each sample was denatured using NaOH (final concentration, 0.2 M) for 10 min at 37 °C, mixed with 30 μl of 10 mM hydroquinone (Wako, Osaka, Japan) and 520 μl of 3 M sodium bisulfite (Nacarai Tesque, Kyoto, Japan), and incubated under mineral oil at 50 °C for 16 h. Modified DNA was purified using a PCR purification kit (Qiagen). The modification was completed by adding NaOH (final concentration, 0.3 M) for 15 min at 37 °C followed by ethanol precipitation. Bisulfite-modified DNA spanning residues from −297 to +104 relative to the transcription start point (15) was amplified, cloned into the TA-vector (Invitrogen), and sequenced using an ABI 377 semiautomatic sequencer (PE Applied Biosystems). At least 10 alleles from each PCR product were sequenced.

Electrophoresis Mobility Shift Assay—Double-stranded DNA fragments corresponding to the sequence from −96 to −69 and −72 to −45 were synthesized by annealing two single-stranded oligonucleotides (5′-GACGAAAGGGGCATCCCGGAGTG-3′ and 5′-CCTGCACTCCCGCATGCCCCCTTT-3′; 5′-CACGACGAGCTTCCCGCGCCGCGA-3′ and 5′-TCTCTCCCGCCGCGGGAAGCTCGT-3′, respectively) and filling in by DNA polymerase I (TOYOBO, Osaka, Japan). These fragments were designated as GR1 and GR2, respectively. C(−52)m^{5}C-GR2 and C(−52)T-GR2 were created using the same method with the exception that cytosine at position −52 in GR2 was substituted with 5-methylcytosine and thymine, respectively. For the formation of the complex, 5 μg of ANOS nuclear extract was incubated with ^{32}P end-labeled oligonucleotides fragments for 20 min at room temperature. The mixtures were electrophoresed in 5% polyacrylamide gel in 0.5% Tris borate EDTA at 45 volts for 3 h, and the gel then was dried and autoradiographed. For the competition assay, the DNA-protein complex was produced in the same way in the presence of the given amounts of non-labeled DNA. In the supershift assay, nuclear extracts were incubated with 1 μg of anti-Sp1 or anti-Sp3 antibody for 1 h on ice before being mixed with labeled DNA.

Luciferase Assay—The 533-bp fragment from −446 to +87 relative to the transcription initiation site of the *ChM-I* gene was amplified by PCR, digested by SacI and XhoI, and cloned into a luciferase reporter plasmid, PGV-B (Toyo Ink, Tokyo, Japan), which was designated PGV-B-f1. The mutant fragment having a thymine residue at position −52 was created by PCR, cloned into PGV-B, and designated PGV-B-mtf1. SL2 cells (5×10^6) were seeded in a 35-mm dish, and 1 μg of each reporter plasmid was co-transfected with 1 μg of the Sp1 (pPacSp1) or Sp3 (pPacSp3 containing a truncated form of Sp3 and pPacUSp3 containing a full-length form of Sp3) expression vector (16) into Schneider cells using EFFECTEN (Qiagen) according to the manufacturer's instructions. Transfection efficiency was standardized by the co-transfection of 1 ng of pRL-TK control vector (Toyo Ink). Cells were harvested 24 h after transfection, and luciferase assays were performed with the PicaGene Dual SeaPansy system (Toyo Ink). Firefly-luciferase activity and SeaPansy-luciferase activity were measured as relative light units with a luminometer (Lumino, STRATEC Biomedical Systems). The firefly-luciferase activity then was normalized for transfection efficiency based on the SeaPansy-luciferase activity. Each experiment was performed in triplicate. Transfection experiments also were performed using ANOS, TAKAO, and primary chondrocytes instead of Schneider cells and the human Sp3 expression vector pRC/CMV/Sp3 (for review see Ref. 16) instead of pPacUSp3.

RNA Interference—RNA interference was achieved using small interfering RNA (siRNA) for the *Sp1* and *Sp3* genes basically as recommended by the manufacturer (Dharmacon). The 21-nucleotide duplexes containing the pattern AA(N19)UU were selected to obtain symmetric 2-nt 3′-overhangs of an identical sequence. Luciferase siRNA duplex (GL2RN1, Dharmacon) was used as a negative control. Transient transfections of siRNAs (1 μg) were performed using Lipofectin 2000 (Invitrogen). RNAs and proteins were prepared 48 h after transfection and used for the RT-PCR and Western blotting.

Chromatin Immunoprecipitation (ChIP)—The suitability of each antibody for the ChIP assay was confirmed by immunoprecipitation-Western blotting assay (data not shown). Cells were harvested and mixed with formaldehyde at a final concentration of 1.0% for 10 min at 37 °C to cross-link protein to DNA. Cells then were suspended in 0.2 ml of SDS lysis buffer and settled on ice for 10 min. DNA cross-linked with protein was sonicated into fragments of 200–1,000 bp. One-tenth of the sample was set aside as an input control, and the rest was precleared with salmon sperm DNA protein A-Sepharose beads (Upstate Biotechnology) for 30 min with agitation. The soluble chromatin fraction was collected with each antibody at 4 °C overnight with rotation. Immune complexes were collected with salmon sperm DNA protein A-Sepharose beads and washed with the manufacturer's low salt, high salt, and LiCl buffers and then washed twice with TE buffer (10 mM Tris-HCl and 1 mM EDTA). The chromatin-antibody complexes were eluted with elution buffer (1% SDS and 0.1 M $NaHCO_3$). Protein DNA cross-links were reversed with 5 M NaCl at 65 °C for 4 h, proteinase K treatment and phenol-chloroform extraction were carried out, and then the DNA was precipitated in ethanol. PCR amplification was performed using primers specific for the *ChM-I* promoter (sense, 5′-GAATGCAGGCCAGTGAGAAGGT-3′; antisense, 5′-GCACCCTGGGATCTGTCCCGCT-3′). The reaction was performed with an initial denaturation of 5 min at 94 °C followed by 30 cycles of 1 min at 94 °C, 1 min at 63 °C, and 1 min at 72 °C with a final extension at 72 °C for 7 min. We confirmed the exponential increase of PCR product at this number of cycles in several preliminary experiments (data not shown).

RESULTS

CBOS Expresses the Cartilage-related Genes—The expression of the *ChM-I* gene along with a number of bone- and cartilage-related genes was analyzed by RT-PCR in 24 OS, and the representative data of 12 cases were presented in Fig. 1*A*. No substantial difference was observed in the expression levels of bone-related genes among three types of OS. As for the cartilage-related genes, however, three subtypes showed a considerable difference. CBOS expressed all of the analyzed carti-

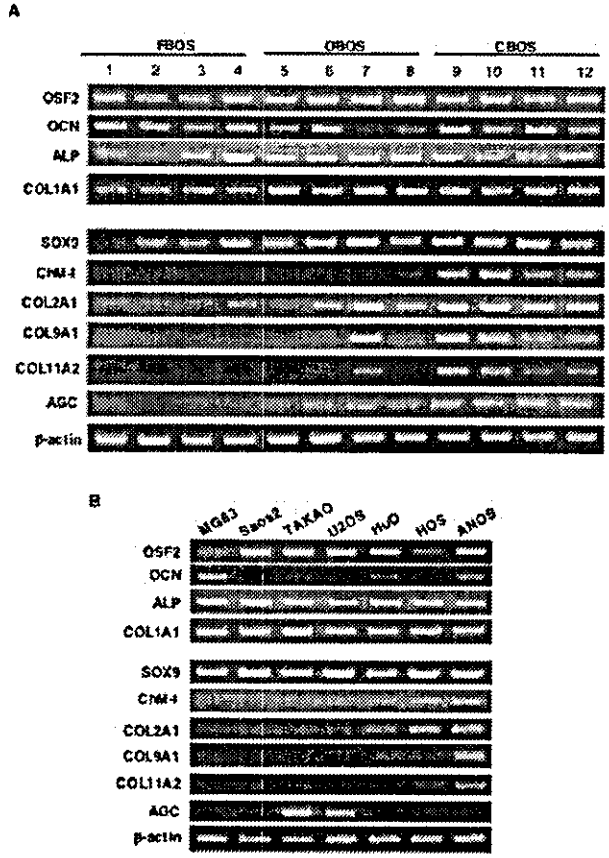

FIG. 1. **Expression of bone- and cartilage-related genes in OS.** mRNA expression of bone-related genes (*OSF2, OCN, ALP,* and *COL1A1*) and cartilage-related genes (*SOX9, ChM-I, COL2A1, COL9A1, COL11A2,* and *AGC*) in primary OS tumors (*A*) and OS cell lines (*B*) were analyzed by RT-PCR.

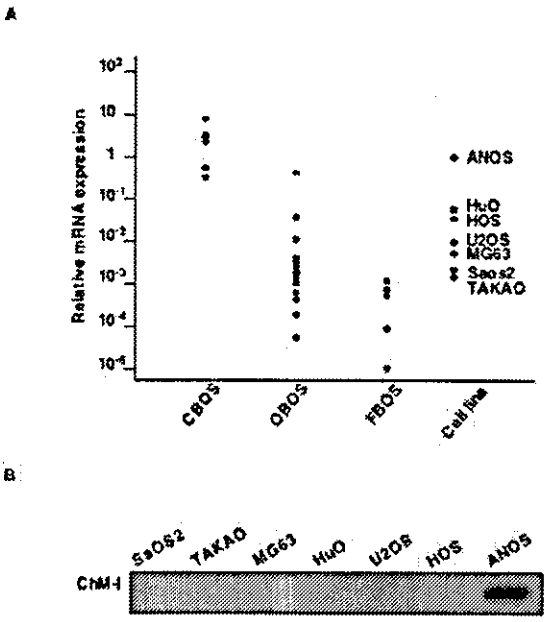

FIG. 2. **Expression of the *ChM-I* in OS.** *A*, quantitative analyses of mRNA expression of the *ChM-I* gene in primary tumors and cell lines. Expression level of the *ChM-I* gene in each sample was demonstrated as a value relative to that in normal cartilage tissue as described under "Experimental Procedures." *B*, Western blot analysis of the ChM-I protein in OS cell lines.

lage-related genes at a high level, whereas none of FBOS expressed *COL9A1, COL11A2,* or *AGC* genes. The expression pattern of the genes in OBOS varied significantly among samples. Interestingly, most of OS irrespective with the histological subtype expressed the *SOX9* gene, whereas the expression of the downstream genes such as *COL2A1* and *AGC* genes showed clear difference among subtypes. The most notable difference between CBOS and other types of OS was the expression of *ChM-I* gene. To confirm that the expression of cartilage-related genes was derived from tumor cells and not from surrounding normal tissues, the expression of the same set of genes was investigated in seven OS cell lines (Fig. 1*B*). All of cartilage-related genes were expressed in ANOS that was established from CBOS. The expression profiles of cartilage-related genes varied significantly among other cell lines. The expression of the *SOX9* gene was observed in all of the cell lines including MG63 and Saos2 in which none of cartilage-related genes other than the *SOX9* was expressed. These data indicated that the expression of the cartilage-related genes in OS stemmed from tumor cells and that some OS tumor cells expressed bone-related genes as well as cartilage-related genes of which the expression was regulated by some mechanisms other than the expression of the *SOX9* gene.

The ChM-I Gene Is Expressed Preferentially in CBOS—The expression of the *ChM-I* gene was analyzed further by quantitative RT-PCR setting the mRNA expression level in normal cartilage as a standard value (1.0). The relative expression level of the *ChM-I* gene in OS samples varied considerably but showed a clear association with the histological subtype (Fig. 2*A*). Most CBOS samples showed a value comparable with that in normal cartilage (0.33–8.15; mean value, 2.58), whereas the expression level in FBOS samples was extremely low (<0.0017). OBOS showed intermediate values with variances among samples (0.8–0.00004) (Fig. 2*A*). The expression level of the *ChM-I* gene in OS cell lines also varied considerably (0.98–0.002) with one cell line, ANOS, having a value (0.98) equivalent to that of the articular cartilage (Fig. 2*A*). ChM-I protein was detected only in ANOS by Western blotting (Fig. 2*B*), suggesting that mRNA expression level similar to that in articular cartilage was required to be detected by Western blotting.

Regulatory Regions of the ChM-I Gene Are Methylated in ChM-I-negative Cells—To investigate the role of epigenetic regulation for the expression of the *ChM-I* gene, the methylation status of the transcription regulatory region of the *ChM-I* gene was analyzed. Yanagihara *et al.* (15) report that the 533-bp region from −487 to +46 relative to the transcription start site contained the major transcription activity of the *ChM-I* gene. Twenty-one CpG sites were found in this region, and the methylation profile of each site was analyzed by bisulfite genomic sequencing (Fig. 3*A*). In normal cartilage cells, the CpG sites in this region were hypomethylated. ANOS in which the expression of the *ChM-I* gene was equivalent to that in normal cartilage cells also showed hypomethylation at the CpG sites from −136 to +15, whereas the CpG sites located further downstream were methylated. In the other six cell lines, the mRNA expression level was correlated with the extent of methylation. The promoter region of Saos2 with no expression of the *ChM-I* gene was methylated extensively, whereas that of HOS with a relatively high level of expression of the *ChM-I* gene was hypomethylated. To investigate whether the methylation in the core-regulatory region was a product of cell culture, the methylation profile in this region was analyzed in the primary tumors of four cases of each subtype (Fig. 3*B*). All of the four CBOSs showed hypomethylation of CpGs in this region, which

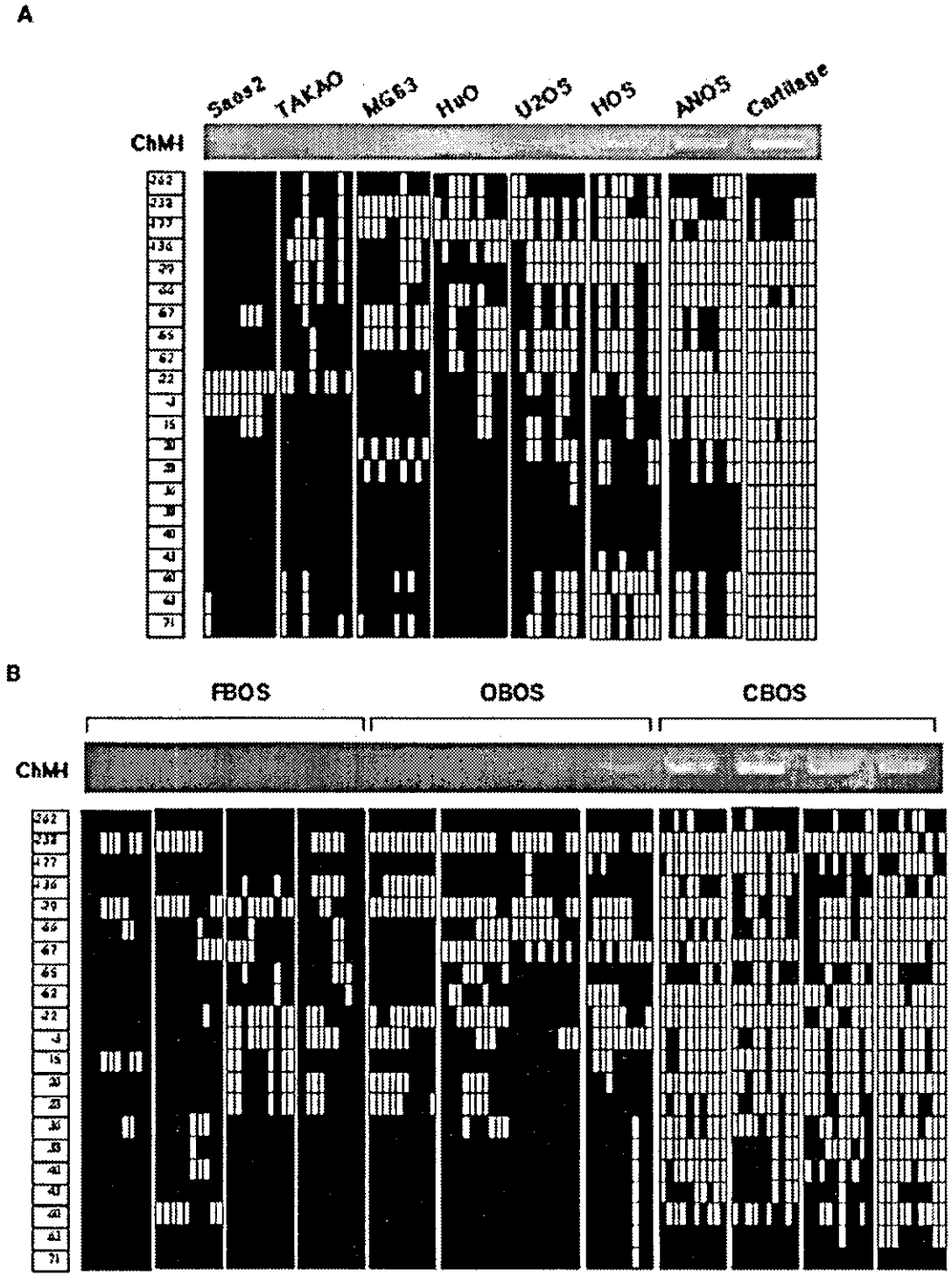

FIG. 3. **Methylation profile of CpG sites in the core-regulatory region of the *ChM-I* gene in OS.** Methylation profiles of OS cell lines (*A*) and primary OS tumors (*B*). Bisulfite genomic sequencing data for 10 alleles in each sample are presented, and *closed* and *open squares* indicate the methylated and non-methylated alleles, respectively. *Numbers* in *boxes* on the *left* indicate the position of each CpG site relative to the transcription start site. The expression of the *ChM-I* gene in each sample detected by standard RT-PCR was demonstrated above the bisulfite genomic sequencing data.

were methylated heavily in all of the FBOSs and OBOSs. These results confirmed that the methylation of the core-regulatory region was not a product of cell culture and was closely associated with the reduced expression of the *ChM-I* gene in primary OS tumors.

Methylation of C(−52) Is Correlated with Reduced Expression of the ChM-I Gene—To further investigate the significance of the methylation as the regulatory mechanism, three cell lines (TAKAO, Saos2, and MG63) showing no expression of the *ChM-I* gene by standard RT-PCR (Fig. 1*B*) were treated with a

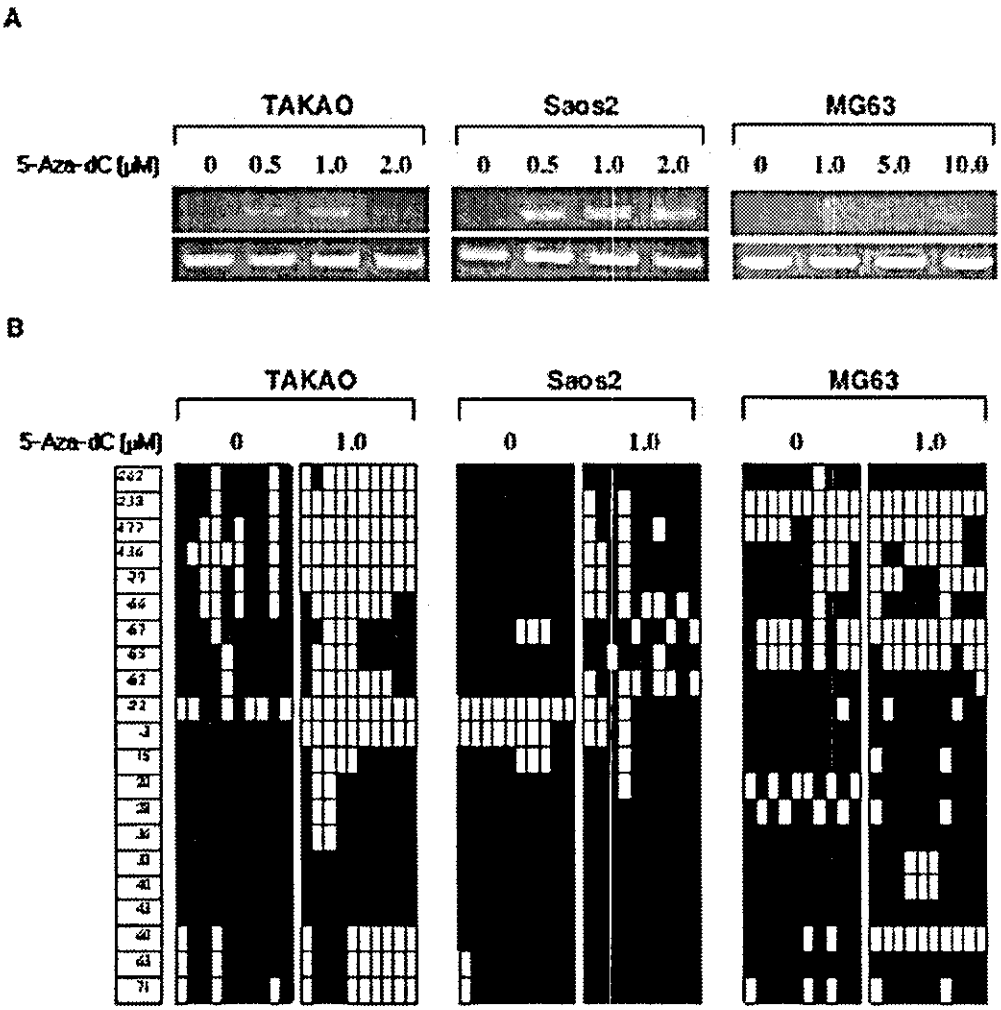

FIG. 4. **Induction of *ChM-I* gene expression by 5-Aza-dC.** *A*, mRNA expression of the *ChM-I* gene in OS cell lines after the treatment with 5-Aza-dC. Cells were incubated with the indicated concentration of 5-Aza-dC for 96 h. *B*, methylation profiles in OS cell lines before and after treatment with 5-Aza-dC. Bisulfite genomic sequencing data for 10 alleles in each sample are presented, and *closed* and *open squares* indicate the methylated and non-methylated alleles, respectively. *Numbers* in *boxes* on the *left* indicate the position of each CpG site relative to the transcription start site.

demethylating agent, 5-Aza-dC. The expression of the *ChM-I* gene was induced in all three cell lines, although MG63 required a much higher concentration of 5-Aza-dC (10 μM) than TAKAO and Saos2 (Fig. 4*A*). Bisulfite genomic sequencing before and after the treatment with 5-Aza-dC (1 μM) showed extensive demethylation in the core-regulatory region in TAKAO and, to a lesser extent, in Saos2 but no demethylation in MG63 (Fig. 4*B*), which was consistent with the level of the *ChM-I* gene expression at this concentration of 5-Aza-dC (Fig. 4*A*). Comparing the methylation profiles at each site before and after the treatment, we found that the methylation of cytosine at −52 (C(−52)) showed a close correlation with the expression of the *ChM-I* gene. Almost all of the alleles of C(−52) in the three cell lines (9/10 in TAKAO, 10/10 in Saos2, and 10/10 in MG63) were methylated before the 5-Aza-dC treatment. After the treatment, 7 and 6 of 10 alleles were free from methylation in TAKAO and Saos2, respectively, whereas only one of ten alleles was demethylated in MG63. In the other OS cell lines and primary OS tumors, the methylation profile of C(−52) was correlated well with the level of expression (Fig. 2, *A* and *B*), suggesting that non-methylated C(−52) is critical for the expression of the *ChM-I* gene in OS cells.

Sp3, but Not Sp1, Binds to the Sp1/3 Binding Site Containing C(−52)—Using TESS (www.cbil.upenn.edu/tess) and TFSEARCH (www. cbil.jp/research/db/TFSEARCH.html), we found that C(−52) was in the middle of the consensus sequence of the Sp1/3 binding site (CGGCGG). To investigate whether this site is a target for the protein binding, a 21-bp oligonucleotides corresponding to −72 to −45 was synthesized (GR2) and used for electrophoresis mobility shift assay with the nuclear extract of ANOS. Electrophoresis mobility shift assay showed that GR2 bound to nuclear protein and that the binding was inhibited by unlabeled GR2 but not by unlabeled GR1 corresponding to −96 to −69, which indicates specific binding (Fig. 5*A*). Both C(−52)m^{5}C-GR2 and C(−52)T-GR2 failed to bind the nuclear extract, indicating that the preservation of a non-methylated C(−52) was critical for the protein binding (Fig. 5*B*). The addition of anti-Sp1 antibody to the GR2-protein mixture had no effect on the GR2-protein binding (Fig. 5*C*). On the other hand, a supershifted band was observed when anti-Sp3 antibody was added to the GR2-protein mixture (Fig. 5*C*), indicating that Sp3 bound to the Sp1/3 site including C(−52) in ANOS. The binding of Sp3 to the core-promoter region *in vivo* was confirmed by ChIP analysis (Fig. 5*D*). Sp3, but not Sp1, bound

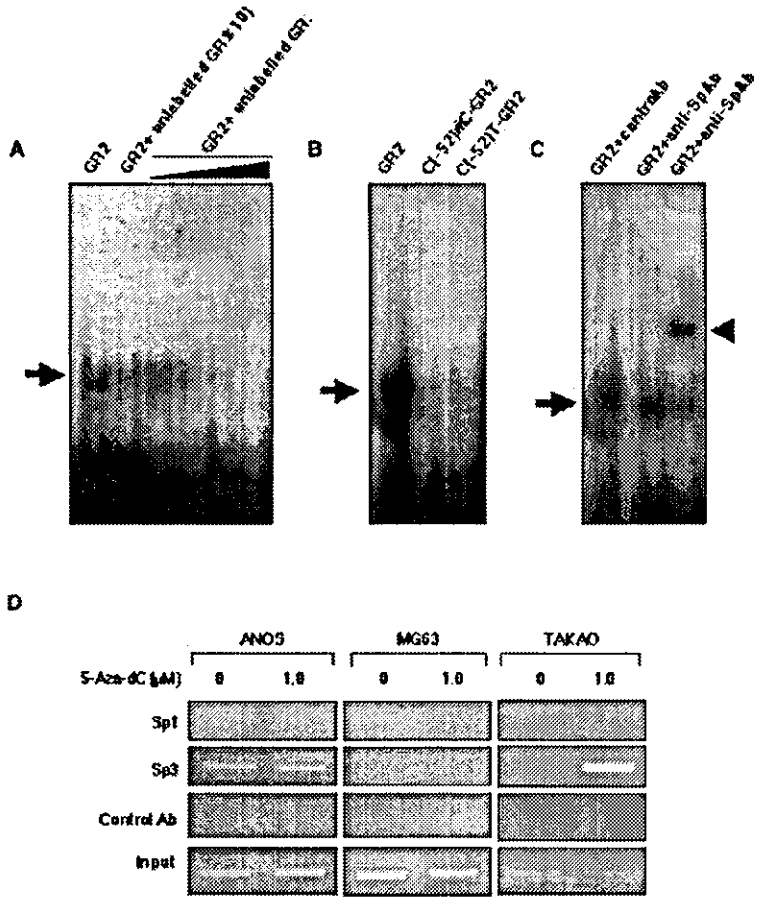

FIG. 5. **Binding of Sp3 to the core-promoter region of the ChM-I gene *in vitro* and *in vivo*.** *A*, specificity of the binding. A 28 bp double-stranded DNA corresponding to the region from −72 to −45 (*GR2*) was radiolabeled and incubated with nuclear extracts of ANOS with the indicated unlabeled competitors. The mixtures were electrophoresed in a 5% polyacrylamide gel, and the gel then was dried and autoradiographed. *Lane 1*, labeled GR2 without competitor; *lane 2*, labeled GR2 with an excess amount (×10) of unlabeled GR1 (corresponding to −96 to −69); *lanes 3–6*, labeled GR2 with unlabeled GR1 (×1, ×2, ×10, and ×100 excess by volume, respectively). The *arrow* indicates the DNA-protein complex. *B*, inhibition of the binding by the replacement of C(−52). GR2 with a methylated C(−52), C(−52)m^{5}C-GR2 (*lane 2*), or with a thymine at −52, C(−52)T-GR2 (*lane 3*), was used instead of GR2. *C*, identification of Sp3 as the protein binding to GR2. Labeled GR2 was preincubated with the indicated antibody before being mixed with nuclear extract of ANOS. *Lane 1*, labeled GR2 preincubated with control antibody (non-immune rabbit IgG); *lane 2*, labeled GR2 preincubated with anti-Sp1 antibody; *lane 3*, labeled GR2 preincubated with anti-Sp3 antibody. The *arrowhead* indicates the supershifted band. *D*, Sp3 binds to the core-regulatory region of the *ChM-I* gene *in vivo*. Cells were treated with/without 5-Aza-dC (1.0 μM) before the DNA-protein complex was formed through treatment with formaldehyde and subjected to a ChIP assay. PCR for the core-regulatory region of the ChM-I gene was performed using DNA extracted from an immunoprecipitated DNA-protein complex using antibodies for Sp1, Sp3, or non-immune rabbit IgG (*Control Ab*).

to the core-promoter region in ANOS. Neither Sp1 nor Sp3 binding was detected in MG63 before or after the treatment with 5-Aza-dC (1.0 μM), whereas Sp3 binding was induced in TAKAO after the treatment with 5-Aza-dC, which was consistent with the results on *ChM-I* gene expression.

Sp3 Up-regulates ChM-I Promoter Activity through the Sp1/3 Sites Containing C(−2)—The Sp1 (pPacSp1) or Sp3 (pPacSp3 or pPacUSp3) expression vector was introduced into SL2 cells with the reporter plasmid containing the wild-type (PGV-B-f1) or mutant (PGV-B-mtf1) fragment (Fig. 6). Co-transfection of PGV-B-f1 with pPacSp1 (Fig. 6*b*) and pPacSp3 (Fig. 6*c*) showed transcriptional activity at a level similar to that obtained with the empty expression vector (pPac) (Fig. 6*a*), whereas pPacUSp3 greatly enhanced the activity (Fig. 6*d*). This induction was abolished completely when PGV-B-mtf1 was used instead of PGV-B-f1 (Fig. 6*h*). These results suggested a positive regulatory role for Sp3 in the ChM-I gene expression, which was mediated by the Sp1/3 site containing C(−52). The induction of the transcription activity of the *ChM-I* gene by Sp3 was analyzed further in OS cell lines and primary chondrocytes (Fig. 7). Transfection of human Sp3 expression vector (pRC/CMV/Sp3) into ANOS (Fig. 7*A*) or primary chondrocytes (Fig. 7*B*), which were positive for the expression of the endogenous *ChM-I* gene, induced the luciferase activity when the reporter plasmids containing the wild-type fragment with C(−52) was co-transfected. The induction level in primary chondrocytes was much lower than that in ANOS, probably because of low transfection efficiency determined by the activity of the control luciferase plasmid, pRL-TK (data not shown). No induction was observed when the reporter plasmids containing the mutant fragment with T(−52) were used. Similar results were observed also in TAKAO (Fig. 7*C*), which was negative for the expression of the endogenous *ChM-I* gene, further suggesting that the expression of endogenous *ChM-I* gene in TAKAO was repressed by methylation at the C(−52) site.

Reduction of the Sp3 Gene Expression Results in the Reduction of the ChM-I Gene Expression—Both Sp1 and Sp3 were expressed in all of the OS cell lines (Fig. 8*A*). To further investigate the role of Sp3 in the expression of the *ChM-I* gene, double-stranded siRNA for *Sp1* or *Sp3* was transfected into *ChM-I*-expressing cells. siRNA for *Sp1* and *Sp3* effectively reduced the mRNA expression of corresponding genes in ANOS, whereas the expression of the *ChM-I* gene was reduced only when the expression of the Sp3 was inhibited (Fig. 8*B*). The expression level of the *ChM-I* gene was confirmed by quantitative RT-PCR, which showed the clear association of siRNA for the *Sp3* with the reduction of the *ChM-I* gene expression (Fig. 8*D*). The effects of siRNA for *Sp1* and *Sp3* were analyzed further at protein level, and again, the reduction of ChM-I protein expression was observed only when the expression of Sp3 was inhibited by siRNA (Fig. 8*F*). Identical results were obtained when human primary chondrocytes were used instead of ANOS. The reduction of Sp3 correlated with the reduction of the *ChM-I* gene at mRNA (Fig. 8, *C* and *E*) and protein level (Fig. 8*G*), suggesting that Sp3 is a positive regulator of the *ChM-I* gene in normal chondrocytes.

DISCUSSION

Cells of the chondrogenic and osteogenic lineages are considered to share mesenchymal stem cells as a common ancestor

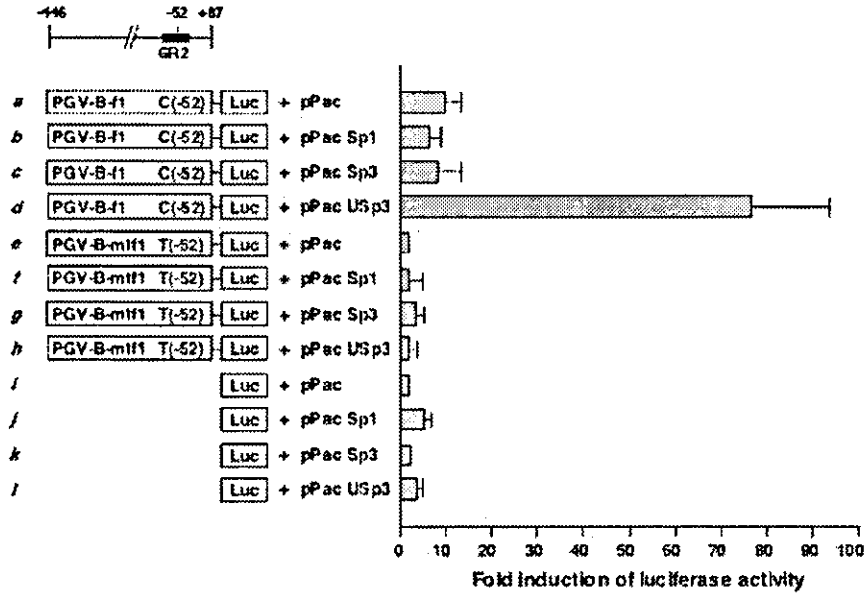

FIG. 6. **Sp3 induces the transcriptional activity of the *ChM-I* gene promoter with C(−52).** The structure of the core-regulatory region of the *ChM-I* gene is demonstrated at the *top* of the figure. *Numbers* indicate positions relative to the transcription start site, and the *thick bar* indicates the Sp1/3 binding site containing C(−52). Luciferase reporter plasmids containing either the wild type (PGV-B-f1) or mutant (PGV-B-mtf1) fragment corresponding to −446 to +87 were co-transfected into SL2 cells with empty vector (pPac), the Sp1 expression vector (pPacSp1), or the Sp3 expression vector (pPacSp3 or pPacUSp3). Results were determined as the fold induction by setting the luciferase activity in the experiments using PGV-B and each construct as 1.0. The mean ± S.D. of three independent experiments is given.

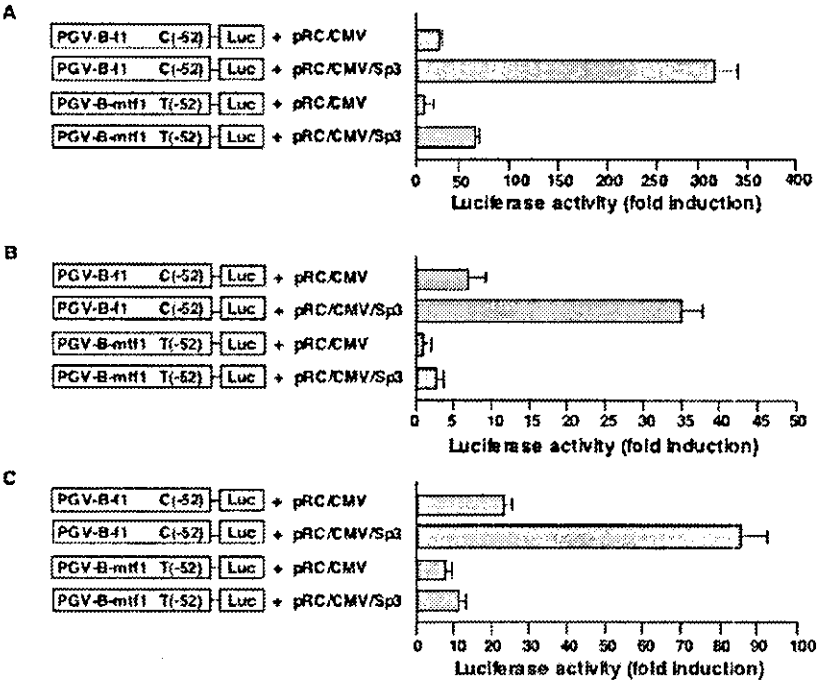

FIG. 7. **Sp3 induces the transcriptional activity of the *ChM-I* gene in OS cell lines and primary chondrocytes.** Luciferase reporter plasmids described in the figure legend of Fig. 6 were co-transfected into ANOS (*A*), TAKAO (*B*), or primary chondrocytes (*C*) with either empty vector (pRC/CMV) or the human Sp3 expression vector (pRC/CMV/Sp3). The results were determined as the fold induction by setting the luciferase activity in the experiments using PGV-B and each construct as 1.0. The mean ± S.D. of three independent experiments is given.

(17, 18), and we and others (19, 20) provide the evidence for the presence of bi-directional precursors, which can differentiate into either chondrogenic or osteogenic cells. In addition to the *ChM-I* gene, CBOS expressed a number of cartilage-related genes such as the *COL2A1*, *COL9A1*, and *AGC* genes (Fig. 1, *A* and *B*), suggesting that CBOS may stem from bi-directional precursors. The expression of "the master gene" has been proposed to regulate the expression of the entire set of genes required for differentiation to specific direction, and in the case of cells of chondrogenic lineage, the *SOX9* has been regarded as such (21). However, all seven OS cell lines expressed the *SOX9* gene irrespective to the expression of downstream genes such as the *COL2A1* gene (Fig. 1*B*) (21). These results suggested the presence of mechanisms to turn off the expression of cartilage-specific genes in OS cells. The results in this study demonstrated an example in which the epigenetic mechanism is involved in such a tissue-specific expression of cartilage-related genes.

Little is known regarding the transcriptional regulation of the *ChM-I* gene. As for extrinsic signals, several growth factors have been shown to reduce the expression of the *ChM-I* gene including fibroblast growth factor-2, transforming growth factor-β, parathyroid hormone, and parathyroid hormone-related peptide (3, 4), but no definite positive regulators for the expression of the *ChM-I* gene are known at present. As for the genomic structures responsible for the transcriptional regulation, Yamagihara *et al.* (15) determine the major regulatory region for the transcription of the *ChM-I* gene and found that the transcription factor YY-1 down-regulated the transcription (15). However, the role of YY-1 *in vivo* was not demonstrated

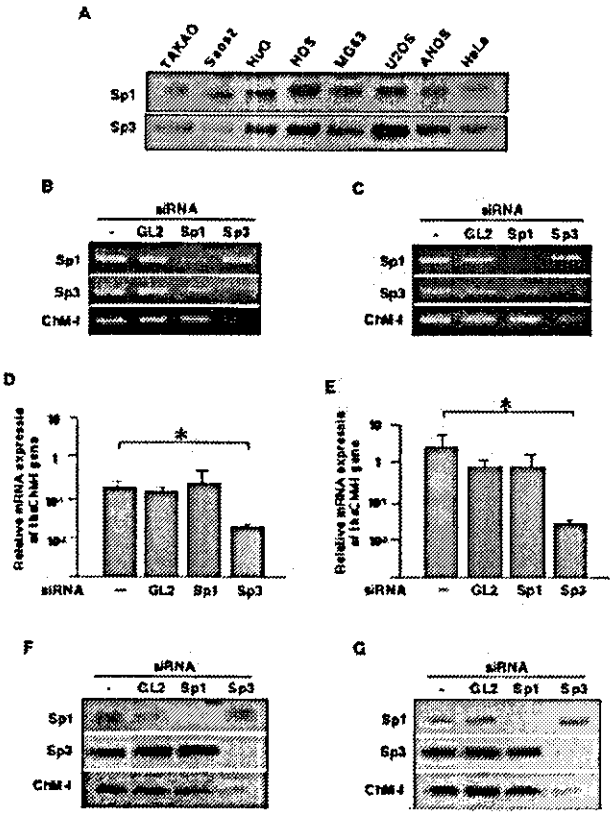

FIG. 8. **Expression of Sp3 associates with the expression ChM-I.** *A*, Western blot analyses of Sp1 and Sp3 in cell lines. *B–G*, inhibition of the Sp3 expression reduced the expression of *ChM-I* gene. siRNA (1 μg) for *Sp1*, *Sp3*, or luciferase (GL2) was transfected into ANOS (*B*, *D*, and *F*) or primary chondrocytes (*C*, *E*, and *G*), and total RNA and protein were extracted at 48 h after the transfection. mRNA expression of *Sp1*, *Sp3*, and *ChM-I* genes was analyzed by the standard RT-PCR (*B* and *C*). The expression of the *ChM-I* gene was evaluated further by quantitative RT-PCR as described under "Experimental Procedures" (*D* and *E*). *, $p < 0.05$. The expression of Sp1, Sp3, and ChM-I protein was analyzed by Western blotting (*F* and *G*).

and the relationship of YY-1 with the down-regulators mentioned above has yet to be proved. In this report, we have shown for the first time that Sp3 is a potent positive regulator of the *ChM-I* gene expression, and the data from the siRNA experiments clearly indicated that Sp3 is a critical factor also in normal chondrocytes. Sp3 is a transcription factor belonging to the Sp1 family, which binds to the consensus GC or GT box (22). Sp3 was isolated as a homologue of Sp1 (23) and reported as the factor that inhibits the function of Sp1 (16). However, evidence is accumulating to suggest that Sp3 also has the ability to stimulate transcription involving the promoters of various genes (24–26), suggesting that Sp3 is a bi-functional transcriptional regulator (24, 27). The studies of Sp3-deficient mice indicate that Sp3 is essential for postnatal survival, late tooth development, and late bone development (28, 29), suggesting its involvement in bone and cartilage metabolism.

Because Sp3 is a transcription factor expressed ubiquitously and indeed all of the OS cell lines expressed Sp3 (Fig. 8*A*), it is reasonable to assume that the binding of Sp3 to the core-promoter region is regulated by some mechanisms that may determine the cell- and stage-specific expression of the *ChM-I* gene. The regulation of higher order chromatin structures by DNA methylation is crucial to tissue-specific gene expression and global gene silencing (30, 31), and we found that the binding of Sp3 was regulated by methylation in the core-regulatory region of the *ChM-I* gene and that treatment with 5-Aza-dC induced the expression of the *ChM-I* gene in association with the binding of Sp3. We have no clear explanation as to why MG63 required a high concentration of 5-Aza-dC to reduce the methylation (Fig. 3*A*). There was no significant difference in the expression of the *Dnmt1* gene among the cell lines (data not shown). Because the growth of MG63 showed no significant change following treatment with 10 μM 5-Aza-dC, which caused severe growth inhibition in all of the other cell lines, there seemed to be a mechanism specific to MG63. Hypermethylation at CpG islands is a common feature of cancer cells (31), and treatments with inhibitors for methyltransferase such as 5-Aza-dC leads to the reactivation of methylation-silenced genes in many cancers (32). Considering these findings, the methylation-associated silencing of the *ChM-I* gene in OBOS and FBOS might be a transformation-related phenomenon. However, it also is likely that the silencing of the *ChM-I* gene is a physiological phenomenon occurring during the differentiation of mesenchymal cells as demonstrated for other genes (33–35). We showed that the removal of methylation restored the binding of Sp3 and induced the expression of the *ChM-I* gene in osteoblastic cells (Fig. 4*B*). However, quantitative RT-PCR revealed that the level of expression was lower than normal level (data not shown), suggesting that the binding of Sp3 is necessary but not enough to gain the full transcriptional activity. The investigation of negative regulators such as YY-1 or other epigenetic regulatory mechanisms such as histone acetylation is required to understand the entire picture of the transcriptional regulation of the *ChM-I* gene.

Acknowledgments—We thank Drs. Y. Hiraki and C. Shukunami for providing anti-human ChM-I antibody, Dr. G. Suske for the Sp1 and Sp3 expression vectors, Dr. T. Uemura for SL2 cells, and the late Dr. M. Oka for continuous and generous support.

REFERENCES

1. Hiraki, Y., Tanaka, H., Inoue, H., Kondo, J., Kamizono, A., and Suzuki, F. (1991) *Biochem. Biophys. Res. Commun.* **175**, 971–977
2. Hiraki, Y., Inoue, H., Iyama, K., Kamizono, A., Ochiai, M., Shukunami, C., Iijima, S., Suzuki, F., and Kondo, J. (1997) *J. Biol. Chem.* **272**, 32419–32426
3. Shukunami, C., Iyama, K., Inoue, H., and Hiraki, Y. (1999) *Int. J. Dev. Biol.* **43**, 39–49
4. Shukunami, C., and Hiraki, Y. (1998) *Biochem. Biophys. Res. Commun.* **240**, 885–890
5. Unni, K. K. (1996) *Dahlin's Bone Tumors*, 5th Ed., Lippincott Williams & Wilkins, Philadelphia
6. Ali, N. H., Harrison, M. A., Rowe, J., and Teich, N. M. (1993) *Bone (NY)* **14**, 847–858
7. Gerstenfeld, L. C., Uporova, T., Schmidt, J., Strauss, P. G., Shih, S. D., Huaman, L. F., Gundberg, C., Mizuno, S., and Glowacki, J. (1996) *Lab. Investig.* **74**, 895–906
8. Murakami, H., Nakayama, T., Nishijo, K., Hosaka, T., Nakamata, T., Aoyama, T., Okamoto, T., Tsuboyama, T., Nakamura, T., and Toguchida, J. (2002) *Cancer Lett.* **182**, 203–211
9. Dorfman, H. D., and Czernisk, B. (1995) *Cancer* **75**, 203–210
10. Li, E. (2002) *Nat. Rev. Genet.* **3**, 662–673
11. Ishii, S., Yamawaki, S., Sasaki, T., Usui, M., Ubayama, Y., Minaimi, A., Yagi, T., Isu, K., and Kobayashi, M. (1982) *Int. Orthop.* **6**, 215–223
12. Hayami, T., Shukunami, C., Mitsui, K., Endo, N., Tokunaga, K., Kondo, J., Takahashi, H. E., and Hiraki, Y. (1999) *FEBS Lett.* **458**, 436–440
13. Kalff-Suske, M., Kunz, J., Grzeschik, K.-H., and Suske, G. (1996) *Genomics* **37**, 410–412
14. Clark, S. J., Harrison, J., Paul, C. L., and Frommer, M. (1994) *Nucleic Acids Res.* **22**, 2990–2997
15. Yanagihara, I., Yamagata, M., Sakai, N., Shukunami, C., Kurahashi, H., Yamazaki, M., Michigami, T., Hiraki, Y., and Ozono, K. (2000) *J. Bone Miner. Res.* **15**, 421–429
16. Hagen, G., Muller, S., Beato, M., and Suske, G. (1994) *EMBO J.* **13**, 3843–3851
17. Caplan, A. I. (1991) *J. Orthop. Res.* **9**, 641–650
18. Prokop, D. J. (1997) *Science* **276**, 71–74
19. Muraglia, A., Cancedda, R., and Quarto, R. (2000) *J. Cell Sci.* **113**, 1161–1166
20. Okamoto, T., Aoyama, T., Nakayama, T., Nakamata, T., Hosaka., T., Nishijo, K., Nakamura, T., Kiyono, T., and Toguchida, J. (2002) *Biochem. Biophys. Res. Commun.* **295**, 354–361
21. de Crombrugghe, B., Lefebvre, V., Behringer, R. R., Bi, W., Murakami, S., and Huang, W. (2000) *Matrix Biol.* **19**, 389–394
22. Suske, G. (1999) *Gene (Amst.)* **238**, 291–300
23. Kingsley, C., and Winoto, A. (1992) *Mol. Cell. Biol.* **12**, 4251–4261
24. Bigger, C. B., Melnikova, I. N., and Gardner, P. D. (1997) *J. Biol. Chem.* **272**, 25976–25982
25. Ihn, H., and Trojanowska, M. (1997) *Nucleic Acids Res.* **25**, 3712–3717

26. Yusa, N., Watanabe, K., Yoshida, S., Shirafuji, N., Shinomura, S., Tani, K., Asano, S., and Sato, N. (2000) *J. Leukocyte Biol.* **68,** 772–777
27. Majello, B., De Luca, P., and Lania, L. (1997) *J. Biol. Chem.* **272,** 4021–4026
28. Bouwman, P., Gollner, H., Elsasser, H. P., Eckhoff, G., Karis, A., Grosveld, F., Philipsen, S., and Suske, G. (2000) *EMBO J.* **19,** 655–661
29. Göllner, H., Dani, C., Phillips, B., Philipsen, S., and Suske, G. (2001) *Mech. Dev.* **106,** 77–83
30. Futscher, B. W., Oshiro, M. M., Wozniak, R. J., Holtan, N., Hanigan, C. L., Duan, H., and Domann, F. E. (2002) *Nat. Genet.* **31,** 175–179
31. Jones, P. A., and Baylin, S. B. (2002) *Nat. Rev. Genet.* **3,** 415–428
32. Karpf, A. R., and Jones, P. A. (2002) *Oncogene* **21,** 5496–5530
33. Locklin, R. M., Oreffo, R. O., and Triffitt, J. T. (1999) *Cell Biol. Int.* **22,** 207–215
34. Ryhanen, S., Pirskanen, A., Jauskelainen, T., and Maenpaa, P. H. (1997) *J. Cell. Biochem.* **66,** 404–412
35. Villagra, A., Gutierrez, J., Paredes, R., Sierra, J., Puchi, M., Imschenetzky, M., Wijnen, Av, A., Lian, J., Stein, G., Stein, J., and Montecino, M. (2002) *J. Cell. Biochem.* **85,** 112–122

JMAM 248
11 February 2005 Disk Used
ARTICLE IN PRESS
No. of Pages 11, DTD = 5.0.1

Available online at www.sciencedirect.com
SCIENCE DIRECT®
Molecular Aspects of Medicine xxx (2005) xxx–xxx
MOLECULAR ASPECTS OF MEDICINE
www.elsevier.com/locate/mam

Review

Mouse models of senile osteoporosis

Ken Watanabe *, Akinori Hishiya

Department of Bone & Joint Disease, National Center for Geriatrics & Gerontology (NCGG), Aichi 474-8522, Japan

Abstract

Little is known about the pathophysiology of normal human and mouse senescence. On the other hand, the pathology of age-related disorders, such as senile osteoporosis, has been investigated. In vivo studies on the pathology of osteoporosis have been conducted primarily in rodents. Although mouse models of senile osteoporosis display some discrepancies relative to their human counterparts with regard to symptoms and pathology, these experimental models are useful and powerful tools for basic and preclinical studies. Here, we review existing mouse models of senile osteoporosis, including those exhibiting premature aging phenotypes, and discuss their pathogenesis, particularly with regard to age-related changes in stem cells.

Contents

* Corresponding author. Tel.: +81 562 46 2311; fax: +81 562 44 6595.
E-mail address: kwatanab@nils.go.jp (K. Watanabe).

0098-2997/$ - see front matter © 2005 Published by Elsevier Ltd.
doi:10.1016/j.mam.2005.01.006

1. Classical models for senile osteoporosis

A decrease in bone mass accompanying advancing age is not specific to humans, but has also been observed in other mammals. Laboratory mice usually live for 2–3 years, and show a peak bone mass at 4–8 months of age, followed by a decline with advanced age. A popular laboratory mouse strain, C57BL/6, develops a senile osteoporosis-like bone phenotype with decreased bone mass and quality (Perkins et al., 1994; Bikle et al., 2002; Cao et al., 2003; Ferguson et al., 2003). Both trabecular and cortical bones suffer dynamic changes with age in this model. Whereas the cancellous bone volume fraction (BV/TV) is significantly decreased from ages 6 weeks to 24 months, cortical thickness is increased until the age of peak bone mass (~6 months), after which it subsequently declines (Bikle et al., 2002). Interestingly, expression of RANKL, also known as osteoclast differentiation factor, is increased with age, correlating with cancellous bone volume (Cao et al., 2003). In another common mouse strain, BALB/c, osteogenic stem cells from 24-month old mice exhibit a decrease in proliferative potential upon aging (Bergman et al., 1996). It is suggested that this age-related bone loss is caused by decreased osteogenic potential due to both quantitative and qualitative declines, especially in stem cell function (Bergman et al., 1996). Additionally, bone marrow hematopoiesis is often affected by aging (Morrison et al., 1996). C57BL/6 mice are known to frequently develop clonal B cell expansion and lymphoma with advanced age (LeMaoult et al., 1999; Ghia et al., 2000). This raises the possibility that age-related, strain-specific hematopoietic disorganization, such as that observed in lymphoma, largely affects bone resorption.

Senescence accelerated mice (SAM) have been established by Takeda et al., and accepted as an appropriate model of aging (Takeda et al., 1997). The SAM lines, derived from the mouse strain, AKR/J, are divided into two classes; P lines exhibit an accelerated aging phenotype with shortened life-span, and R lines show a relatively less accelerated phenotype. The aging phenotype of P lines becomes apparent at 6–8 months of age. Among the SAM lines, SAM-P6 has been utilized as a model for human senile osteoporosis, and characterization of the resultant bone phenotype has been well described (Matsushita et al., 1986; Jilka et al., 1996; Kajkenova et al., 1997; Silva et al., 2002). Jilka et al. (1996) demonstrated that the osteopenic phenotype was caused by reduced osteoblastogenesis and that bone metabolism was resistant to gonadectomy. Furthermore, increased adipogenesis and myelopoiesis have been observed in bone marrow from the mice (Kajkenova et al., 1997). In addition, the long bones in SAM-P6 were longer but more fragile than those in controls (Silva et al., 2002). With these and other numerous reports of in vivo and ex vivo studies with the SAM-P6 model, a number of phenotypic characteristics, thought to be consistent between aging mice and humans, have been observed. It should be noted, however, that some controversial observations and/or interpretations, probably due to their complicated genetic backgrounds, have also been described. Because the SAM strains are polygenic, those specific genetic factors accounting for the observed bone phenotypes are still awaiting elucidation.

2. Premature aging syndromes in genetically modified mice

As described above, aged animals appear to be good models for senile osteoporosis. However, the mechanisms underlying the aging process are complex, making it difficult to decipher at the molecular level. Using knockout or transgenic techniques, some of these genetically modified mice result in premature aging phenotypes. The significant conclusion to be taken from these studies is that single gene mutations cause multiple aging phenotypes. This advantage is useful in the search for clues to the regulation of bone metabolism during the aging process (Hishiya and Watanabe, 2004).

Mouse models for human progeroid syndromes have also been reported (Kuro-o, 2001; Hasty et al., 2003; Warner and Sierra, 2003; Hasty and Vijg, 2004; Kipling et al., 2004). Genetically modified mice, which exhibit multiple aging phenotypes and shortened life span, are listed in Table 1. Werner syndrome is caused by a loss-of-function mutation in *WRN*, which encodes the RecQ family DNA helicase, and plays a role in genome stability, including telomere maintenance (Yu et al., 1996). Unexpectedly, knockout mice for the *Wrn* gene are essentially normal and exhibit no characteristics of premature aging (Lombard et al., 2000). These mice have long telomeres and relatively high telomerase activity, suggesting that the aging phenotype is latent as a result of residual telomere maintenance activity. Evidently, double knockout mice for *Wrn* and *Terc*, which encode the RNA component of telomerase activity, show a Werner-like phenotype with osteoporosis (Chang et al., 2004; Du et al., 2004). Recently, a gene encoding lamin A has been identified to be responsible for the human progeria, Hutchinson-Gilford syndrome (De Sandre-Giovannoli et al., 2003; Eriksson et al., 2003). Mice carrying an autosomal recessive point mutation in the lamin A gene, corresponding to the mutation identified in humans, also develops a progeria-like phenotype with osteoporotic symptoms (Mounkes et al., 2003).

Besides these authentic models for human premature aging syndromes, mice presenting with multiple aging phenotypes have also been reported. Null mutations of the Ku86 gene, also known as Ku80, which plays a role in DNA repair and transcription, exhibits shortened life span and elicits a premature aging phenotype, including osteopenia (Vogel et al., 1999). The aging phenotype has been also observed in mice lacking PASG, an SNF-like molecule that functions in DNA methylation (Sun et al., 2004). Mutant mice show decreased BMD and a secondary ossification delay in the tibial epiphyses (Sun et al., 2004). In addition to the genetic mutations involved in genomic stability and nuclear organization, mice carrying mitochondrial DNA polymerase mutations, resulting in loss of the region responsible for its proofreading activity, also show the osteoporotic phenotype along with other premature aging symptoms (Trifunovic et al., 2004); in particular, decreased bone mass, which is now known and appreciated as a hallmark of the premature aging phenotype. However, most observations of the skeletal phenotype were examined by X-ray analysis. The pathophysiology, including histology, of the bone phenotypes in these models for premature aging has not been well described, as yet.